Research Square

Preprints are preliminary reports that have not undergone peer review.
They should not be considered conclusive, used to inform clinical practice,
or referenced by the media as validated information.

Adjunctive Cystic Duct Ligation Refines the Murine Bile Duct Ligation Model of Portal Hypertension

Qi Zhao
Changzheng Hospital, Naval Medical University
Hai-Lin Xiong
The First Affiliated Hospital, Jiangxi Medical College, Nanchang University
Xin Zhang
Changzheng Hospital, Naval Medical University
Wei-Fen Xie
weifenxie@medmail.com.cn
Changzheng Hospital, Naval Medical University

Method Article

Keywords: portal hypertension, bile duct ligation, cystic duct ligation, liver fibrosis

Posted Date: November 10th, 2026

DOI: https://doi.org/10.21203/rs.3.rs-11365837/v1

License: This work is licensed under a Creative Commons Attribution 4.0 International License.
Read Full License

Additional Declarations: No competing interests reported.

Abstract

Background

Murine bile duct ligation (BDL) is widely used to model cholestatic liver injury and portal hypertension (PH), but postoperative complications and mortality undermine its experimental utility. We examined whether adjunctive cystic duct ligation (CDL) improves survival while preserving the portal hypertensive phenotype. Male C57BL/6J mice underwent sham surgery, conventional BDL, or the refined BDL + CDL procedure. Four-week survival was compared among groups. Portal pressure was assessed in independent terminal cohorts at 1, 2, 3, and 4 weeks post-surgery. Systemic hemodynamics, organ-to-body weight ratios, liver fibrosis, and biochemical injury markers were comprehensively evaluated.

Results

The refined BDL + CDL group showed markedly improved postoperative survival at four weeks compared with the BDL group (56.1% vs. 28.3%; hazard ratio, 0.490; 95% confidence interval, 0.304–0.790; log-rank *P* = 0.003). BDL + CDL reduced the incidence of postoperative complications, particularly gallbladder perforation and ascites. In addition, the BDL + CDL procedure induced a more severe and progressive PH, with portal pressure significantly higher than that in the BDL group. The exacerbated PH was associated with aggravated intrahepatic fibrosis, evidenced by advanced histopathological staging, increased collagen deposition, pro-fibrogenic molecular signature, and elevated liver injury markers. Mean arterial pressure and heart rate did not differ significantly among groups.

Conclusions

Incorporating CDL into the standard BDL procedure establishes a more robust and reproducible experimental model for studying PH. This refined model offers translational utility for investigating PH pathophysiology and evaluating novel anti-fibrotic therapies.

Background

Portal hypertension (PH), characterized by a sustained pathological increase in portal venous pressure, is a pivotal pathophysiological manifestation and a central determinant of hepatic decompensation [1, 2]. It imposes a substantial clinical burden, worsens patient prognosis and quality of life, and strains healthcare resources [3, 4]. Despite intensified research efforts and the emergence of promising therapeutic candidates, liver transplantation remains the only definitive treatment, underscoring the persistent challenge of translating preclinical discoveries into clinical benefit [4, 5]. Bridging this gap depends on preclinical studies that use animal models to explore disease mechanisms, identify new therapeutic targets, and evaluate potential interventions before clinical application. The value of such models rests on how faithfully and reproducibly they recapitulate the hemodynamic and

histopathological hallmarks of PH, as these properties largely determine the translational relevance of experimental findings.

Available preclinical models of PH engage distinct pathogenic compartments and therefore capture different facets of the human disease. Prehepatic models, such as partial portal vein ligation (PPVL), elevate portal pressure rapidly but cause no intrinsic liver injury and fail to replicate the intrahepatic fibrosis that defines clinical cirrhosis. By contrast, toxin-induced models (e.g., thioacetamide and carbon tetrachloride) and cholestatic models permit the study of PH in the setting of parenchymal injury and tissue remodeling, albeit with prolonged induction periods or higher perioperative morbidity [6, 7]. Among these, bile duct ligation (BDL) is widely used because it reproducibly induces cholestatic fibrosis and PH within approximately 2–3 weeks and is adaptable across species [7, 8].

Traditionally, rats were the preferred species for BDL-based PH research owing to their larger size and greater procedural feasibility [6]. The advent of sophisticated genetic tools, which enable transgenic, knockout, and conditionally targeted manipulations, has shifted the field decisively toward genetically tractable mouse models, which are now indispensable for mechanistic and translational studies [7, 8]. The transition to mouse models, however, introduces practical challenges. The small size of mice renders BDL technically more demanding and amplifies the risk of perioperative complications, such as gallbladder distension, perforation, and bile leakage (unlike rats, which anatomically lack a gallbladder), leading to biliary peritonitis or sepsis [6, 7]. Reported survival after BDL varies widely across studies, ranging from early mortality of > 20% [9] to 70% mortality within the first postoperative week [10] and, ultimately, death of all animals within 7–10 weeks [7]. This variation reflects differences in the research objectives of BDL models (e.g., acute obstructive jaundice, chronic cholestasis, or PH), the observation windows, and operative factors such as ligation-site variability and the resulting degree of common bile duct obstruction [11]. Thus, refining the BDL procedure in mice is essential to fully realize the potential of this model in PH research.

After conventional BDL in mice, the gallbladder remains in continuity with the obstructed biliary tree and progressively distends with bile, predisposing it to perforation and leakage. To address this morbidity, we hypothesized that adjunctive cystic duct ligation (CDL), by excluding the gallbladder from continued biliary inflow, would reduce distension-related complications while maintaining extrahepatic obstruction and preserving model stability. Here, we show that this refinement substantially improves survival and reduces complications, providing a more robust and reproducible platform for PH research.

Methods

Animals

Eight-week-old male C57BL/6J mice (20–25 g) were obtained from Sippe-Bk Lab Animal Co., Ltd (Shanghai, China). Mice were housed in a specific pathogen-free (SPF) animal facility under a controlled 12-hour light/dark cycle and had free access to standard rodent chow and water. All experimental

protocols were approved by the Animal Ethics Committee of The Second Affiliated Hospital of Naval Medical University and performed in accordance with the ARRIVE 2.0 guidelines.

Murine BDL and BDL + CDL procedures

After one week of acclimation, mice were randomly assigned using a computer-generated randomization sequence to three groups: sham-operated control, conventional BDL, and refined BDL + CDL. All surgical procedures were performed under aseptic conditions by the same experienced operator to minimize technical variability; outcome assessment was performed by investigators blinded to group allocation. Anesthesia was induced and maintained with isoflurane, and ophthalmic lubricant was applied to both eyes during surgery. Each mouse was placed in a supine position on a heating pad maintained at 37°C. After shaving and disinfection of the abdominal skin with chlorhexidine gluconate and 75% alcohol, a 1.5–2.0 cm midline laparotomy was performed to expose the hepatic portal triad.

The common bile duct, identified as a thin whitish tubular structure coursing between the portal vein and the hepatic artery, was gently dissected from the adjacent vasculature and connective tissue with fine micro-serration forceps and cotton-tipped swabs, maintaining the duct intact while avoiding injury to the portal vein. Extrahepatic cholestasis was induced by double ligation of the common bile duct with two non-absorbable 5 − 0 silk sutures: the proximal ligature was placed at the upper end of the common bile duct, distal to the confluence of the hepatic ducts and the cystic duct, and the distal ligature at the lower end of the common bile duct, proximal to the insertion of the pancreatic duct. The duct was not transected between the ligatures, thereby minimizing bile extravasation and the risk of subsequent chemical peritonitis.

In animals assigned to the refined BDL + CDL group, an additional cystic duct ligation was performed immediately after the bile-duct ligation and before abdominal closure. The gallbladder was exposed by gentle retraction of the overlying liver lobe. The cystic duct was carefully dissected free from the adjacent liver parenchyma and periductal connective tissue using fine forceps, with care taken to avoid puncture of the gallbladder wall. A single non-absorbable 5–0 silk suture was then placed around the cystic duct, thereby excluding the gallbladder from the obstructed biliary tree while leaving the gallbladder in situ (Fig. 1).

Sham-operated controls underwent an identical laparotomy with the same exposure and gentle manipulation of the portal triad and gallbladder but without any duct ligation. Postoperatively, all mice were recovered on a warming pad and provided supportive care and analgesia in accordance with institutional animal-care guidelines. Animals were monitored daily for signs of distress and wound healing. Mice were euthanized at 1, 2, 3, and 4 weeks after surgery with 5–6 mice per group per time point, for terminal physiological measurements and tissue collection. Portal pressure at different time points was obtained from independent terminal cohorts rather than from repeated measurements in the same animals.

Measurement of portal pressure

Mice were anesthetized with isoflurane (5% for induction, 2% for maintenance) delivered through a facemask and positioned supine on a thermostatic platform maintained at 37°C. A heparinized 27-gauge catheter was inserted into the ileocolic vein at an approximately 30° angle and advanced approximately 1.0 cm. After stable blood backflow was observed, the catheter was secured and connected to an ALCB10 pressure transducer (Shanghai ALC Biotechnology, China). Pressure waveforms were recorded continuously for 5 min using ALC-MPA software (version 2.1.6), and mean portal pressure was calculated from stable recording segments. The catheter and transducer lines were flushed with heparinized saline before measurement. This measurement was performed at an ambient temperature of 25°C.

Measurement of mean arterial pressure and heart rate

Mean arterial pressure (MAP) and heart rate (HR) were assessed using the ALC-NIBP non-invasive blood pressure system with an ALCB10 amplifier and ALC-MPA software (Shanghai ALC Biotechnology Co., Ltd., China). Mice were placed in a custom acrylic restraint on a heating pad to maintain a core temperature of 37.0 ± 0.5°C. A flexible piezoresistive cuff was positioned 5 mm proximal to the site of strongest pulsation on the tail artery and connected to the amplifier. After a 10-minute acclimation period, the cuff was inflated to 180 mmHg at a rate of 15 mmHg/s to occlude arterial flow, held for 5 seconds, and then deflated at 20 mmHg/s. Oscillometric wave amplitudes and pulse intervals were recorded. Systolic blood pressure (SBP) was defined as the pressure at which the oscillation amplitude reached 50% of its maximum, and diastolic blood pressure (DBP) as the pressure at which the amplitude decreased to 80%. MAP was calculated as MAP = DBP + (SBP - DBP)/3, and HR was derived from the intervals between pulse peaks. Three consecutive measurements were obtained at 5-min intervals, and the average MAP and HR values were used for analysis.

Serum biochemistry

After portal pressure measurements, blood was collected from the portal vein and centrifuged at 3,000 rpm for 15 min at 4°C to obtain serum. Total bilirubin (TBIL), alanine aminotransferase (ALT), and aspartate aminotransferase (AST) were measured using commercial assay kits (Nanjing Jiancheng, China) according to the manufacturer's instructions. Each sample was analyzed in duplicate.

Histology and immunostaining

Liver tissues were fixed in 4% paraformaldehyde, embedded in paraffin, and sectioned at 4 μm. Sections were stained with hematoxylin and eosin (H&E) to assess tissue architecture, and Sirius Red staining was used for collagen visualization [10]. Sirius Red-positive area was quantified using ImageJ (National Institutes of Health, USA) and expressed as a percentage of total tissue area. Fibrosis was assessed

independently by two blinded observers using the METAVIR framework [12]: F0, no fibrosis; F1, portal fibrosis without septa; F2, portal fibrosis with few septa; F3, numerous septa without cirrhosis; and F4, cirrhosis.

For immunohistochemistry and immunofluorescence staining, deparaffinized and rehydrated sections were blocked for 1 h in phosphate-buffered saline containing Tween 20 (PBST) and 5% bovine serum albumin, followed by incubation with primary antibodies overnight at 4°C. After washing, sections were incubated with appropriate secondary antibodies for 1 hour. For immunofluorescence staining, nuclei were counterstained with DAPI, and images were captured using a Leica confocal microscope. Antibody information is provided in Additional file 1: Table S2.

Hydroxyproline analysis

Hepatic collagen content was assessed by quantifying hydroxyproline levels using a commercial Hydroxyproline Assay Kit (STA-675; Cell Biolabs, San Diego, CA) according to the manufacturer's protocol. The measured hydroxyproline content was normalized to the wet weight of the liver tissue and expressed as μg/mg wet tissue.

RNA extraction and quantitative real-time PCR

Total RNA was extracted from liver tissue samples using TRIzol® Reagent (Takara, Tokyo, Japan). RNA purity and concentration were assessed with a NanoDrop 2000 spectrophotometer (Thermo Fisher Scientific, USA). For cDNA synthesis, total RNA (2 μg) was reverse transcribed using MMLV Reverse Transcriptase (Fermentas, USA) and oligo (dT) primers. Quantitative real-time PCR (qRT-PCR) was performed using TB Green® Premix Ex Taq™ II (Takara Bio Inc., Japan) on a StepOnePlus™ Real-Time PCR System. Amplification specificity was confirmed by melt-curve analysis. Relative gene expression levels were calculated using the $2 - \Delta\Delta Ct$ method [13] and normalized to Gapdh as an internal control. Primer sequences were designed and validated using NCBI Primer-BLAST; details are provided in Additional file 1: Table S1.

Western blotting

Liver tissues were homogenized in lysis buffer (5% SDS, 25% glycerol, 125 mM Tris-HCl, pH 6.8, 1 mM PMSF) and then centrifuged to remove debris. Protein concentration was determined using a BCA Protein Assay Kit (Beyotime Biotechnology, China). Equal amounts of protein were separated by SDS-PAGE and subsequently transferred to nitrocellulose membranes (HAHY00010, Millipore) under constant current. The membranes were blocked with 5% non-fat milk in PBST for 1 h at room temperature and incubated overnight at 4°C with specific primary antibodies. Following washes with PBST, membranes were incubated with IRDye®-conjugated secondary antibodies for 1 hour. Protein bands were visualized

using Odyssey® CLx imaging system (LI-COR Biosciences, USA) in the 700- or 800-nm channel. Primary antibody information is provided in Additional file 1: Table S2.

Statistical analysis

All statistical analyses were performed using GraphPad Prism 10 Software (San Diego, CA, USA). Data are presented as mean ± standard deviation (SD). Survival differences were analyzed using Kaplan-Meier curves and the log-rank test, with hazard ratios calculated by Cox proportional hazards regression. For comparisons between two groups, the unpaired Student's t-test was used for normally distributed data, and the Mann-Whitney U test was applied for non-normally distributed data. One-way analysis of variance (ANOVA) was used for comparisons among multiple groups involving one independent variable, and two-way ANOVA was used for datasets with two independent variables. *P* value < 0.05 was considered statistically significant.

Results

Adjunctive cystic duct ligation improves postoperative survival and reduces BDL-associated complications in mice

To determine whether adjunctive CDL improves postoperative survival and reduces BDL-associated complications, a total of 117 adult male C57BL/6J mice were randomly assigned to conventional BDL (n = 60) or the refined BDL + CDL procedure (n = 57). An additional sham-operated cohort served as a non-cholestatic surgical control, and no deaths were observed in the sham group. All animals were monitored longitudinally for four weeks after surgery, and survival was analyzed using the Kaplan–Meier method. Although the two survival curves were broadly comparable during the first postoperative week, a marked divergence emerged from the second week onward (BDL vs. BDL + CDL: 50.0% vs. 70.2%) and remained distinct through the third week (40.0% vs. 64.9%), suggesting that the excess mortality associated with conventional BDL occurs predominantly in the early-to-mid postoperative period rather than during the immediate perioperative phase. This temporal pattern indicates that the later survival difference is not attributable to the operative procedure itself, given that mortality in the first few postoperative days was similar between groups. By 4 weeks, survival was 56.1% in the BDL + CDL group versus 28.3% in the conventional BDL group, corresponding to approximately half the hazard of death (hazard ratio = 0.490; 95% confidence interval, 0.304–0.790; *P* = 0.003; Fig. 2A).

Postmortem examination and terminal anatomical assessments revealed a lower incidence of major procedure-related complications in BDL + CDL mice. Compared with conventional BDL, the BDL + CDL group exhibited a lower incidence of gallbladder perforation and ascites (Fig. 2B). These findings are consistent with the established complication profile of conventional BDL, in which perioperative bile leakage and secondary sepsis contribute substantially to early mortality, and progressive ascites develops in a considerable proportion of animals [6, 7]. Accordingly, the low 4-week survival of

conventional BDL reflects its established morbidity burden, whereas the survival advantage of BDL + CDL is consistent with a contribution from reduced postoperative complications rather than from a less severe disease model. Taken together, these data support BDL + CDL as a useful platform for long-term studies of PH, in which reduced attrition permits a more complete longitudinal assessment of disease progression.

The refined BDL + CDL model produces a stronger portal hypertensive phenotype

Portal pressure, the principal hemodynamic readout of BDL-induced portal hypertension [6], was measured in independent cohorts at 1, 2, 3, and 4 weeks after surgery to determine whether CDL altered the core portal hypertensive phenotype. Both BDL and BDL + CDL groups showed a progressive rise in portal pressure that exceeded that in sham controls from 2 weeks onward. The BDL and BDL + CDL groups did not differ significantly at week 1, and showed only a numerical difference at 2 weeks (P = 0.059); from 3 weeks onward, however, portal pressure in BDL + CDL mice was significantly higher than in conventional BDL mice, and the between-group gap widened progressively through 4 weeks (Fig. 3A). This temporal course parallels the classical evolution of BDL-induced PH, in which portal pressure rises with the progressive accumulation of biliary fibrosis [7, 8].

Consistent with a more pronounced portal hypertensive state, BDL + CDL mice also showed a trend toward a higher liver-to-body weight ratio (0.0780 vs. 0.0688; P = 0.0711) and a significantly higher spleen-to-body weight ratio (0.0096 vs. 0.0079; P = 0.0116) than BDL controls (Fig. 3B, C), indicating aggravated hepatomegaly and splenomegaly. These organ-level changes corroborate the portal pressure measurements and suggest that BDL + CDL yields a more severe and progressive portal-hypertensive phenotype for subsequent mechanistic studies.

Exacerbated portal hypertension in BDL + CDL is driven by hepatic fibrosis rather than systemic hemodynamic changes

The pathophysiology of cirrhotic portal hypertension is classically conceptualized as the sum of increased intrahepatic vascular resistance and elevated splanchnic blood flow, as described by the backward and forward flow theories [14]. To elucidate the mechanisms underlying the more severe PH observed in BDL + CDL mice, we examined both systemic hemodynamics and hepatic structural remodeling at 3 weeks after surgery, a time point at which the BDL-induced portal hypertensive phenotype is already well established [7, 8].

PH in cirrhosis is frequently accompanied by a hyperdynamic circulatory state; we therefore measured MAP and HR as principal indices of systemic hemodynamic involvement. At the 3-week endpoint, neither MAP nor HR differed significantly among the sham, BDL, and BDL + CDL groups (Fig. 4B). Because no

significant differences were detected in these systemic parameters, we next assessed whether enhanced hepatic fibrosis was associated with the aggravated PH in BDL + CDL mice. Histological examination with hematoxylin and eosin (H&E) staining revealed more pronounced architectural distortion and bile duct proliferation in BDL + CDL livers, while Sirius Red staining revealed more extensive collagen deposition and bridging fibrosis in the refined model (Fig. 4C). In line with the established temporal progression of biliary fibrosis—which evolves from portal-based disease to bridging septal fibrosis—the BDL + CDL group exhibited more extensive septal bridging and a higher overall fibrosis burden. The distribution of METAVIR stages confirmed this qualitative impression, with the majority of BDL mice displaying predominantly F1–F2 fibrosis, whereas a larger proportion of BDL + CDL mice reached F3-stage fibrosis (Fig. 4D).

Quantitative biochemical and molecular analyses substantiated these histological findings. Hepatic hydroxyproline content was significantly higher in BDL + CDL mice than in BDL controls (0.172 ± 0.012 vs. 0.151 ± 0.011 μg/mg; $P = 0.0246$) (Fig. 4E), accompanied by an increased collagen fraction on Sirius Red staining, a larger COL1A1-immunopositive area, and a broader α-SMA-positive region by immunofluorescence staining (Fig. 4C). At the transcriptional level, qRT-PCR revealed a coordinated pro-fibrogenic program, characterized by marked upregulation of *Acta2, Col1a1, Col3a1*, and *TIMP1*, together with downregulation of the matrix-degrading protease *MMP9* (Fig. 4F). Western blotting showed increased α-SMA and COL1A1 protein abundance in BDL + CDL livers (Fig. 4G), providing evidence of fibroblast activation and matrix deposition at the protein level. Biochemically, serum ALT, AST, and TBIL also tended to be higher in BDL + CDL than in BDL mice, consistent with more severe hepatobiliary injury and cholestasis (Fig. 4H).

Taken together, these data indicate that the aggravated PH in BDL + CDL is driven primarily by hepatic fibrosis, with no detectable difference in systemic hemodynamics. This refined model therefore provides a more severe, fibrosis-dependent portal hypertensive phenotype and constitutes a robust platform for mechanistic studies of PH.

Discussion

The BDL model remains one of the most widely used platforms for studying cholestatic liver disease and PH [7, 8]. In the present study, adding CDL to conventional BDL improved postoperative survival, reduced complications, and produced a more pronounced portal hypertensive phenotype in mice. Higher portal pressure at later assessments was accompanied by greater hepatic fibrosis, whereas the systemic hemodynamic indices remained similar among groups. These findings support CDL as a potentially useful modification when the experimental objective requires sustained cholestatic injury and directly measurable PH.

From an anatomical perspective, this survival benefit can be explained by exclusion o the gallbladder from the biliary circuit. As outlined above, the gallbladder acts as a low-pressure reservoir that progressively fills with bile and is vulnerable to pressure-related ischemic injury, with subsequent

perforation, leakage, and secondary peritonitis; excluding it therefore removes an important source of late postoperative death. These observations establish an association between reduced perforation and improved survival, but cause-specific mortality was not quantified, and the relative contribution of individual complications to the survival difference therefore remains to be determined.

Beyond procedural feasibility, BDL + CDL produced a stronger portal hypertensive phenotype than conventional BDL, with higher portal pressures and greater hepatosplenomegaly. This combination—reduced mortality together with aggravated liver disease—may appear counterintuitive, but both follow from the same modification: excluding the gallbladder prevents its delayed perforation while while maintaining biliary obstruction and intrahepatic cholestasis. By reducing early mortality among the most severely affected animals, BDL + CDL may limit survivorship bias and thus provide a more reliable platform for longitudinal and pharmacological studies.

Portal pressure reflects the interaction of portal inflow and vascular resistance [15]. Systemic hemodynamics, as reflected by MAP and HR, did not differ among sham, BDL, and BDL + CDL groups, providing no support for a hyperdynamic circulatory contribution at this stage, although these measures do not exclude regional splanchnic or portal venous changes. Because intrahepatic fibrosis is the principal determinant of the elevated hepatic resistance that drives PH, the parallel increases in fibrosis and portal pressure in BDL + CDL mice support a fibrosis-driven mechanism [16, 17]. We propose that exclusion of the gallbladder reservoir could alter biliary pressure and bile-acid exposure, thereby intensifying biliary injury and fibrogenesis [18, 19]. Bile acids are increasingly recognized not merely as cholestasis markers but as signaling mediators that can directly promote PH [20–22], providing a plausible link between CDL-augmented cholestasis and heightened portal pressure.

Several limitations should be acknowledged. Follow-up was limited to 4 weeks, so whether the survival advantage of BDL + CDL is maintained over longer periods, when cholestatic injury and PH continue to progress, remains to be determined. Portal pressure was assessed in independent terminal cohorts, whereas detailed fibrosis and systemic hemodynamic assessments were concentrated at a single endpoint; the temporal sequence of these changes therefore cannot be established. METAVIR staging was developed for human chronic hepatitis and provides a descriptive framework here rather than a validated staging system for murine cholestatic injury. Finally, the model was established and validated in male C57BL/6J mice and requires validation across sexes, strains, and operators.

Conclusions

In summary, adding CDL to the standard BDL procedure yields a refined PH model that simultaneously improves 4-week survival and reduces postoperative complications after BDL, while increasing hepatic fibrosis and portal pressure. By curtailing perioperative losses and amplifying fibrosis-associated PH, BDL + CDL offers a practical, reproducible, and translationally relevant tool for investigating PH pathophysiology and evaluating candidate therapies.

Abbreviations

PH
portal hypertension
BDL
bile duct ligation
CDL
cystic duct ligation
PPVL
partial portal vein ligation
α-SMA
alpha-smooth muscle actin
ALT
alanine aminotransferase
AST
aspartate aminotransferase
TBIL
total bilirubin
COL1A1
collagen type I alpha 1
MMP9
matrix metalloproteinase 9
TIMP1
tissue inhibitor of metalloproteinases 1
DAPI
4',6-diamidino-2-phenylindole
SBP
systolic blood pressure
DBP
diastolic blood pressure
H&E
hematoxylin and eosin
HR
heart rate
MAP
mean arterial pressure
qRT-PCR
quantitative real-time polymerase chain reaction
PMSF
phenylmethylsulfonyl fluoride

SDS-PAGE
sodium dodecyl sulfate–polyacrylamide gel electrophoresis

Declarations

Ethics approval and consent to participate

All animal protocols were approved by the Animal Ethics Committee of The Second Affiliated Hospital of Naval Medical University(approval number: TJCB00120101) and were conducted at the specific pathogen-free animal facility of the Naval Medical University Animal Laboratory Center.

Consent for publication

Not applicable.

Competing interests

The authors declare no competing interests.

Funding

This work was supported by the National Key R&D Program of China (2023YFC2507500 to Wei-Fen Xie).

Author Contribution

QZ and WFX conceived and designed the study. QZ and HLX performed the experiments and data analyses. QZ drafted the manuscript. XZ assisted with the formal analysis and provided resources. WFX provided resources and supervision, and revised the manuscript critically. All authors have read and approved the final version of the manuscript.

Acknowledgements

Not applicable.

Data Availability

The datasets generated and analyzed during the current study are available from the corresponding author on reasonable request.

References

1. de Franchis R, Bosch J, Garcia-Tsao G, Reiberger T, Ripoll C, Baveno VII. Faculty. Baveno VII - Renewing consensus in portal hypertension. J Hepatol. 2022;76(4):959–74.
2. Baveno VIII, Faculty. Baveno VIII - Advancing consensus in portal hypertension. J Hepatol. 2026. Epub ahead of print.
3. Huang DQ, Terrault NA, Tacke F, Gluud LL, Arrese M, Bugianesi E, et al. Global epidemiology of cirrhosis - aetiology, trends and predictions. Nat Rev Gastroenterol Hepatol. 2023;20(6):388–98.
4. Abraldes JG, Trebicka J, Chalasani N, D'Amico G, Rockey DC, Shah VH, et al. Prioritization of Therapeutic Targets and Trial Design in Cirrhotic Portal Hypertension. Hepatology. 2019;69(3):1287–99.
5. Gracia-Sancho J, Marrone G, Fernández-Iglesias A. Hepatic microcirculation and mechanisms of portal hypertension. Nat Rev Gastroenterol Hepatol. 2019;16(4):221–34.
6. Nevzorova YA, Boyer-Diaz Z, Cubero FJ, Gracia-Sancho J. Animal models for liver disease - A practical approach for translational research. J Hepatol. 2020;73(2):423–40.
7. Geerts AM, Vanheule E, Praet M, Van Vlierberghe H, De Vos M, Colle I. Comparison of three research models of portal hypertension in mice: macroscopic, histological and portal pressure evaluation. Int J Exp Pathol. 2008;89(4):251–63.
8. Tag CG, Sauer-Lehnen S, Weiskirchen S, Borkham-Kamphorst E, Tolba RH, Tacke F et al. Bile duct ligation in mice: induction of inflammatory liver injury and fibrosis by obstructive cholestasis. J Vis Exp. 2015;(96):52438.
9. Faccioli LAP, Dias ML, Paranhos BA, Dos Santos Goldenberg RC. Liver cirrhosis: An overview of experimental models in rodents. Life Sci. 2022;301:120615.
10. Aoki H, Aoki M, Yang J, Katsuta E, Mukhopadhyay P, Ramanathan R, et al. Murine model of long-term obstructive jaundice. J Surg Res. 2016;206(1):118–25.
11. Tang G, Nierath WF, Leitner E, Xie W, Revskij D, Seume N, et al. Comparing animal well-being between bile duct ligation models. PLoS ONE. 2024;19(7):e0303786. 10.1371/journal.pone.0303786.
12. López-De León A, Rojkind M. A simple micromethod for collagen and total protein determination in formalin-fixed paraffin-embedded sections. J Histochem Cytochem. 1985;33(8):737–43.
13. Bedossa P, Poynard T. An algorithm for the grading of activity in chronic hepatitis C. The METAVIR Cooperative Study Group. Hepatology. 1996;24(2):289–93.
14. Livak KJ, Schmittgen TD. Analysis of relative gene expression data using real-time quantitative PCR and the 2(-Delta Delta C(T)) method. Methods. 2001;25(4):402–8.
15. Zhang J, Huo Y, Bian J, Cha L, Yang Q, Zhao C, et al. Multimodal assessment of liver stiffness and portal hemodynamics in a cirrhotic mouse model. Front Bioeng Biotechnol. 2026;14:1888436.
16. Sikuler E, Groszmann RJ. Interaction of flow and resistance in maintenance of portal hypertension in a rat model. Am J Physiol. 1986;250(2 Pt 1):G205–12.
17. Friedman SL. Hepatic stellate cells: protean, multifunctional, and enigmatic cells of the liver. Physiol Rev. 2008;88(1):125–72.

18. Wei Q, Li M, Yang Q, Ren M, Liu X, Cai X, et al. Targeting FGG alleviates cholestatic fibrosis by inhibiting hepatic stellate cell activation and regulating macrophage homeostasis. J Nanobiotechnol. 2026;24(1):525.
19. Myung SJ, Yoon JH, Gwak GY, Kim W, Yang JI, Lee SH, et al. Bile acid-mediated thrombospondin-1 induction in hepatocytes leads to transforming growth factor-beta-dependent hepatic stellate cell activation. Biochem Biophys Res Commun. 2007;353(4):1091–6.
20. Sánchez-Sánchez P, Wang Z, Zagorac S, Domínguez M, Boskovic J, Nair A, et al. FXR-YAP signalling maintains biliary epithelial cell identity and preserves liver homeostasis. Nat Metab. 2026;8(5):1189–211.
21. Xiong HL, Zhao Q, Liu SQ, Chen LL, Nie MT, Hong XL, et al. Rifaximin ameliorates cirrhotic portal hypertension through suppression of microbiome-derived deoxycholic acid. J Hepatol. 2026;85(3):515–27.
22. Zang Y, Shi J, Zhao G, Tang B, Liu M, Yao B, et al. A first-in-class pulsatile FXR agonist for bile-acid-related liver diseases. Nature. 2026;655(8123):758–68.

Additional File

Table S1
Primer sequences for qRT-PCR

Gene	Primer	Sequences
Mouse gapdh	Forward	5’- CACCATGGAGAAGGC – 3’
	Reverse	5’- GACGGACACATTGGGGGTAG – 3’
Mouse Acta2	Forward	5’- CTGTCCCTCTATGCCTCTGG – 3’
	Reverse	5’- AGGGCTGTGATCTCCTTCTG – 3’
Mouse Col1a1	Forward	5’- TAAAGGGTCATCGTGGCTTC – 3’
	Reverse	5’- GACGGCTGAGTAGGGAACAC – 3’
Mouse Col3a1	Forward	5’- GCTGATGATGCTGGCTACTG – 3’
	Reverse	5’- AGCAGGTCTGTGTCTTCCTG – 3’
Mouse TIMP1	Forward	5’-ATTCAAGGCTGTGGGAAATG-3’
	Reverse	5’-GATGTGCAAATTTCCGTTCC-3’
Mouse MMP9	Forward	5’- CAATCCTTGCAATGTGGATG – 3’
	Reverse	5’- AGTAAGGAAGGGGCCCTGTA – 3’

Table S2
Antibody details

Antibodies	Source	Identifier
Anti-α-SMA (rabbit)	Bioss	Cat# bs-10196R
Anti-α-SMA (mouse)	Dako	Cat # DK2600
Anti-Col1A1 (rabbit)	Bioss	Cat # bs-10423R
Anti-Col1A1 (rabbit)	Cell Signaling Technology	Cat#72026
anti-GAPDH (mouse)	ABclonal	Cat # AC033
Alexa Fluor™ 546(mouse)	Thermo Fisher	Cat# A10036

Figures

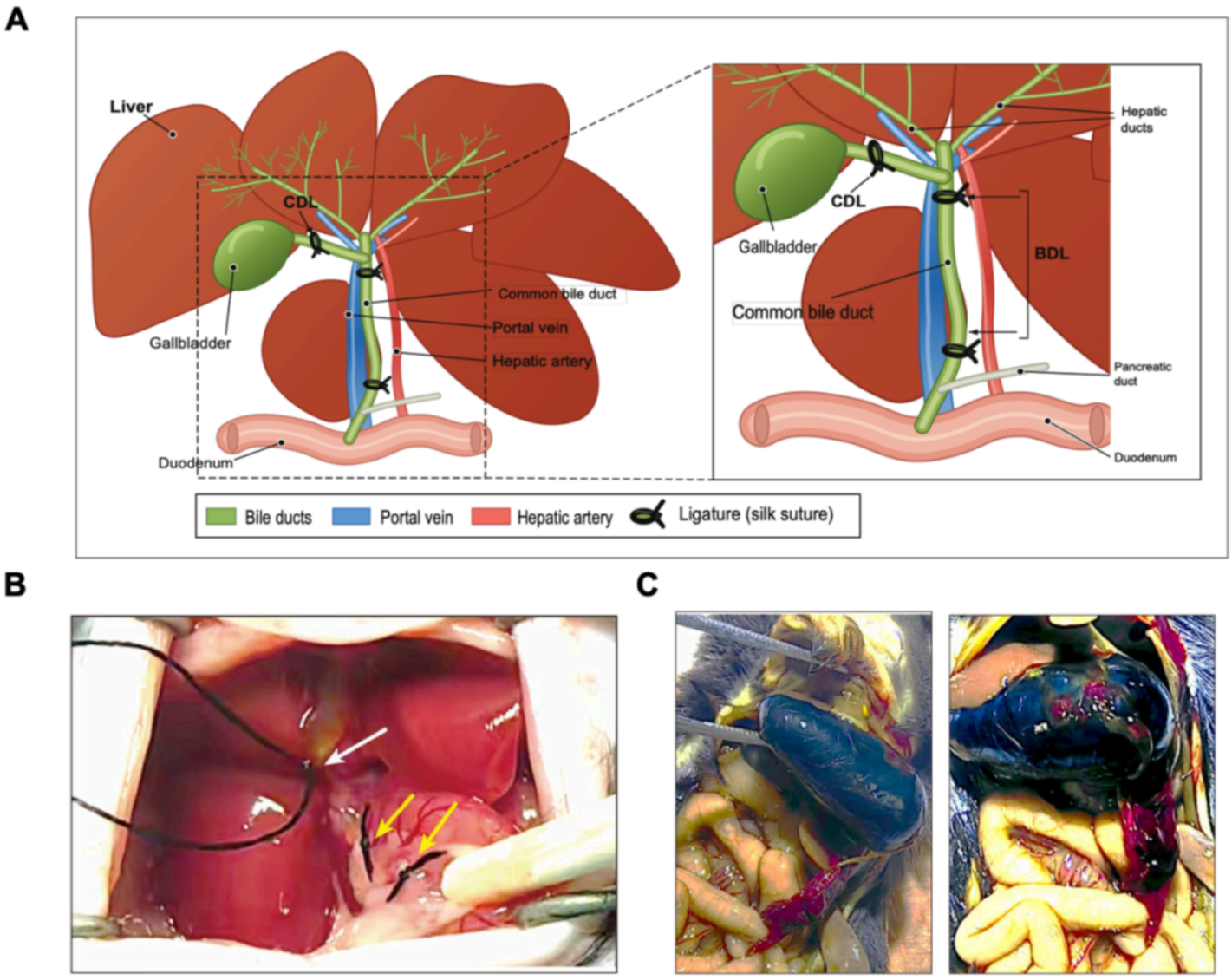


Figure 1

Schematic of the refined BDL+CDL surgical procedure and representative postoperative complication of conventional BDL. (A) Schematic of the murine hepatobiliary anatomy illustrating the ligation sites of the refined BDL+CDL procedure. The gallbladder is retained in situ but excluded from the biliary tree. (B) Intraoperative photograph showing double ligation of the common bile duct (yellow arrows) and additional ligation of the cystic duct (white arrow). (C) Representative photograph showing gallbladder distension and perforation after conventional BDL.

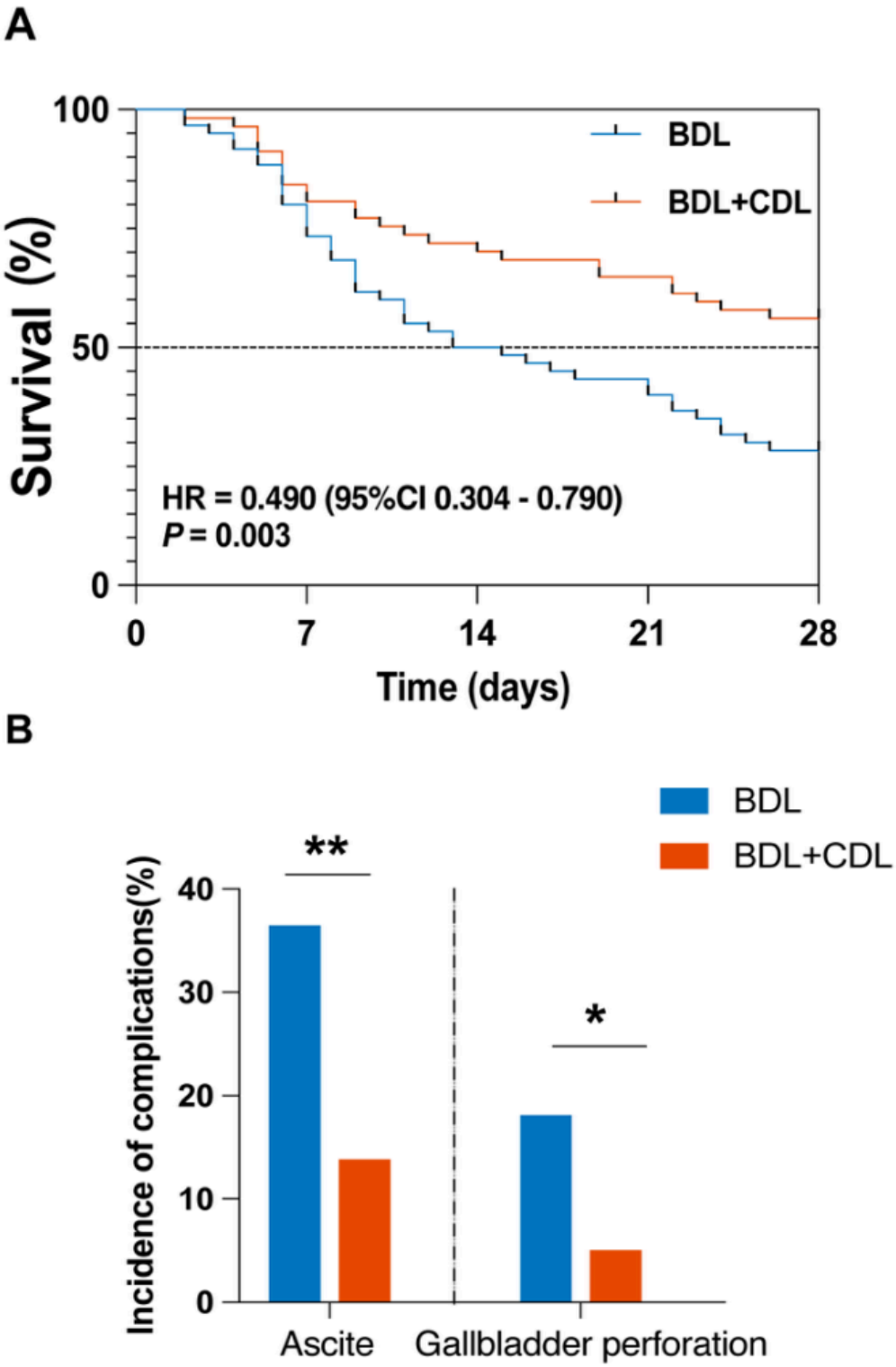


Figure 2

Adjunctive CDL improves survival and reduces major perioperative complications in BDL mice. (A) Kaplan–Meier survival curves of conventional BDL (n=60) and BDL+CDL (n=57) mice over the four-week postoperative period. Survival curves diverged from the second postoperative week, culminating in a significantly higher cumulative survival in the BDL+CDL group (56.1%, 32/57) than in the BDL group (28.3%, 17/60). Log-rank test, *P*= 0.003. (B) Bar graphs comparing the incidence of gallbladder

perforation and ascites between the BDL and BDL+CDL groups. Data are presented as percentages. *P < 0.05, **P < 0.01 (Fisher's exact test).

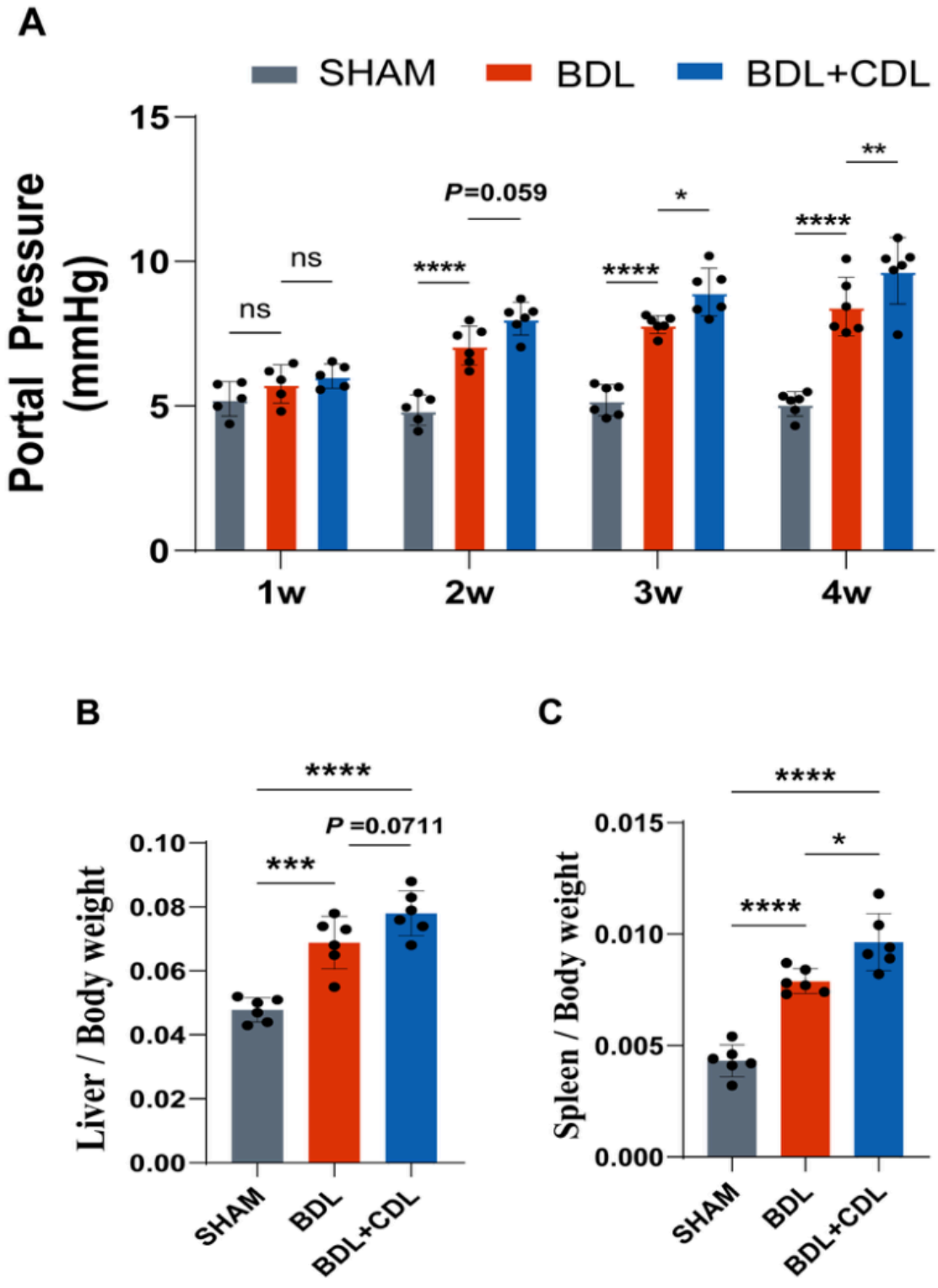


Figure 3

Portal hypertensive phenotype after BDL and BDL+CDL. (A) Serial portal pressure measurements in independent sham, BDL, and BDL+CDL cohorts at weeks 1, 2, 3, and 4 after surgery (n = 5–6 per group

per time point). (B, C) Liver-to-body weight ratio (B) and spleen-to-body weight ratio (C) at week 3 post-surgery (n = 6 per group). Data are presented as mean ± SD. Statistical analysis was performed using one-way ANOVA. *P < 0.05; **P < 0.01; ***P < 0.001; ****P< 0.0001.

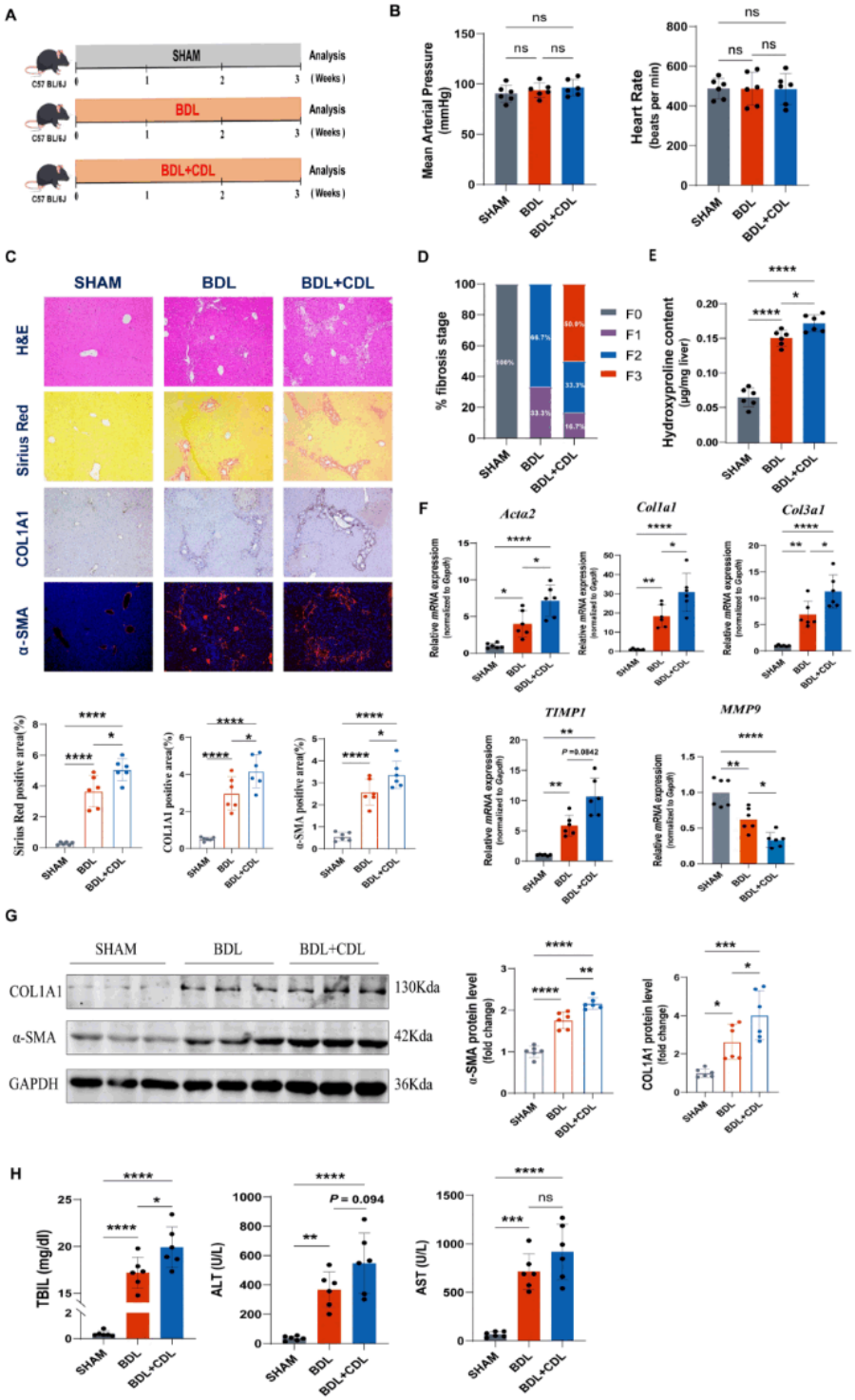


Figure 4

Assessment of hepatic fibrosis and systemic hemodynamics in the refined portal hypertension (PH) model. (A) Schematic illustration of the experimental protocol for BDL-induced PH (n=6 per group). (B) Systemic hemodynamic parameters at the 3-week time point. (Left) Mean arterial pressure (MAP). (Right) Heart rate (HR). (C) Representative images of liver sections stained with hematoxylin and eosin (H&E), Sirius Red, COL1A1 (immunohistochemistry) and α-SMA (immunofluorescence). Scale bars, 100 μm. Semi-quantitative analysis of collagen, α-SMA, and COL1A1 deposition is shown. (D) Distribution of Metavir fibrosis stages among Sham, BDL, and BDL+CDL groups. (E) Hepatic hydroxyproline content as a quantitative measure of collagen. (F) Relative mRNA expression of hepatic fibrosis-related genes (*Acta2, Col1a1, Col3a1, TIMP1,* and *MMP9*). (G) Western blotting analysis and quantification of COL1A1 and α-SMA protein expression in liver tissues**.**(H) Serum levels of total bilirubin (TBIL), alanine aminotransferase (ALT), and aspartate aminotransferase (AST). Data with error bars represent the means ± SD and were analyzed by one-way ANOVA. *$P < 0.05$, **$P < 0.01$, ***$P < 0.001$. ****$P < 0.0001$; ns, not significant.

Supplementary Files

This is a list of supplementary files associated with this preprint. Click to download.

- supplementaryfile.docx